On the Applications of the Finite Element Method in Unsteady Aerodynamics

THEODORE BRATANOW* AND AKIN ECER†
University of Wisconsin at Milwaukee, Milwaukee, Wis.

Treatment of difficulties related to the application of the finite element method for numerical solutions of the Navier-Stokes equation is discussed. The unsteady flow around a stationary and an oscillating NACA 0012 airfoil was analyzed. In an effort to establish the range of applicability of the developed numerical method, the accuracy and stability problems in representing unsteady flow patterns and determining pressure distribution around the airfoil were investigated. Errors involved in determining the velocity field and in the numerical integration of the discretized form of the vorticity transport equation were analyzed in terms of geometry of the finite element gridwork, boundary conditions for stationary and oscillating airfoils, angles of attack, and flow conditions.

Nomenclature

A = area of the region including the airfoil and the surrounding flow
H = height of a triangular element in Fig. 3, in. (m)
H_b = thickness of the boundary layer, in. (m)
N = conditioning number of a matrix
t = time, sec
$\mathbf{u}$ = velocity vector, $\mathbf{u} = [u \quad v]$, in./sec (m/sec)
u_i, v_i = velocity in x and y directions at the nodes of the finite element gridwork, in./sec (m/sec)
$\mathbf{W}$ = vector representing the vorticities at the nodes of the finite element gridwork
$d\mathbf{W}/dt$ = vector representing the rate of change in vorticities at the nodes of the finite element gridwork
x_{ij}, y_{ij} = difference in x and y coordinates between two nodal points of a finite element, in. (m)
δ = vector representing Lagrangian multipliers
Δt = time step in numerical integration, sec
$\Delta\mathbf{X}, \Delta\mathbf{S}, \Delta\mathbf{T}$ = perturbation in matrices $\mathbf{X}$, $\mathbf{S}$, $\mathbf{T}$
λ = eigenvalue of matrix $\mathbf{S}_\omega$
λ_i = eigenvalue matrix $S_\omega{}^e$ of a finite element triangle in Eq. (29)
μ_i = eigenvalues of matrix $\mathbf{S}_s$
ν = kinematic viscosity, in.^{2}/sec (m^2/sec)
ψ = stream function
$\mathbf{\Psi}$ = vector representing stream function and velocities
ω = vorticity, 1/sec
Ω = area of triangular element, in.^{2} (m^2)
∇ = del operator
∇^2 = Laplace operator

Subscripts

s = for stream function and velocities
x, y = for the derivatives with respect to x and y
ω = for vorticities
o = at time t_o
H = at the upper corner of the triangular element
v = viscous
c = convective

Superscripts

e = for a finite element
t = transpose

Presented at the AIAA Computational Fluid Dynamics Conference, Palm Springs, Calif., July 19–20, 1973; submitted July 16, 1973; revision received November 29, 1973. This research was supported by NASA under Grant NGR-50-007-001.

Index category: Nonsteady Aerodynamics.

* Professor of Engineering Mechanics. Member AIAA.

† Assistant Professor of Engineering Mechanics. Member AIAA.

Introduction

NUMERICAL solutions of the Navier-Stokes equation have attracted much attention in recent years. The finite-difference method has been the popular tool for such solutions.[1,2] Finite-difference solutions for the flow problem past a circular cylinder, for instance, have been presented by many authors.[3–5] On the over-all, most of the developed procedures were designed for specific applications and become impractical for large scale problems that require a detailed representation. For these cases, the numerical errors become especially important. The accuracy and stability of numerical solutions of the Navier-Stokes equation, as obtained by finite-difference methods, have been investigated by several authors.[6–8] The importance of convective terms[9] and the boundary conditions[10] has been studied in terms of the finite-difference discretization of this equation.

The application of the finite element method for the solution of the Navier-Stokes equation has been presented by several authors.[11–14] The over-all objectives of the investigation in Refs. 13 and 14 were the determination of pressure distribution and unsteady flow patterns around pitching and plunging airfoils. The finite element method was applied in the analysis for the development of the mathematical formulation and the numerical procedure in a general manner. The various parameters in the analysis can easily be distinguished—the velocity field was calculated at each time step; the time-dependent equation was given in terms of vorticity only; and the boundary conditions were separated from the remainder of the formulation. Time and space discretization can be easily distinguished. Each portion of the formulation can be studied separately, and causes of accuracy and stability problems can be investigated. The classical procedures of error analysis can be used in the solution of the linear system of equations and the numerical integration of the system of equations, since the entire formulation was expressed in terms of matrix algebra.

This paper presents a treatment of the computational difficulties involved in the application of the finite element method for the analysis of unsteady flow around moving obstacles using the numerical method described in Refs. 13 and 14. The accuracy and stability of the developed numerical method are discussed in terms of the basic mathematical formulation and the specific application of the method for analysis of unsteady flow around a NACA 0012 airfoil.

A complete treatment of the sources of numerical errors and instability problems is essential in the application of numerical methods. In analyzing a particular flow around an obstacle, one has to make decisions regarding the finite element gridwork, the discrete representation of the obstacle, the accuracy of the

discretization functions, the numerical integration technique, the choice of the time steps in the numerical integration, etc. In the following, the importance of geometric, kinematic, and physical components of the analysis in obtaining accurate and stable results was evaluated. An attempt was made to establish a range of applicability of the presented numerical method[13] for a larger class of problems.

Summary of the Mathematical Procedure

By introducing stream functions and vorticities, the Navier-Stokes equation for two-dimensional, unsteady, incompressible flow can be written as the vorticity transport equation in the following form:

$$(\partial\omega/\partial t)+(\mathbf{u}\cdot\nabla)\omega = \nu\nabla^2\omega \tag{1}$$

The vorticities and stream functions are defined as

$$-\omega = \nabla^2\psi \tag{2}$$

and

$$\mathbf{u} = [(\partial\psi/\partial y)\ (-\partial\psi/\partial y)] \tag{3}$$

For a specific set of boundary conditions, the solution of Eqs. (1) and (2) can be obtained using a variational formulation by minimizing the following two functionals

$$\Phi_1 = \int_A \omega\frac{\partial\omega}{\partial t}dA + \frac{1}{2}\int_A [u\omega\omega_x + v\omega\omega_y]\,dA + \frac{\nu}{2}\int_A [\omega_x^2+\omega_y^2]\,dA \tag{4}$$

$$\Phi_2 = \tfrac{1}{2}\textstyle\int_A [\psi_x^2+\psi_y^2]\,dA - \int_A \omega\psi\,dA \tag{5}$$

Equation (5) is the exact variational formulation of the Poisson's equation. However, Eq. (4) is developed by linearizing the convection terms in Eq. (1) from a Taylor series expansion of the velocity field, at a time when the vorticities are changed by $d\omega$ as

$$\psi = \psi_0 + (\partial\psi/\partial\omega)_0\,d\omega + \tfrac{1}{2}(\partial^2\psi/\partial\omega^2)_0(d\omega)^2 + \cdots \tag{6}$$

where the velocities can be calculated from Eq. (3). Further details of the variational formulation are given in Refs. 13 and 14. The variational functionals in Eqs. (4) and (5) represent the undisturbed flow without the obstacle. The boundary conditions for the moving obstacle were introduced in these two equations, at each time step of the numerical integration, using the Lagrangian multiplier technique as external constraint conditions. The solutions of both equations were selected from functions which satisfy the boundary conditions. The details of the application of the Lagrangian multiplier technique were presented in Refs. 13–15.

The variational functionals of Eqs. (4) and (5) were then discretized in finite element form using discrete approximation functions for each of the triangular elements of the gridwork shown in Fig. 1. To obtain a consistent solution for each triangular element, a linear variation of vorticities and third-order variation of stream functions were assumed. The resulting discretized variational functionals were minimized. Details of the derivation of the finite element models and the resulting matrix equations are given in Refs. 13 and 14.

The finite element discretization of Eq. (5) yields a system of linear algebraic equations as follows

$$\begin{bmatrix}\mathbf{S}_s & \mathbf{b}_s\\ \mathbf{b}_s^t & \mathbf{0}\end{bmatrix}\begin{bmatrix}\boldsymbol{\Psi}\\ \boldsymbol{\delta}_s\end{bmatrix} = \begin{bmatrix}\mathbf{h}_s\\ \mathbf{e}_s\end{bmatrix} \tag{7}$$

In Eq. (7) the matrix $\mathbf{S}_s$ is formulated for a flow space without the obstacle using the finite element method. The directions of the streamlines and the zero velocity conditions were specified at a series of points on the airfoil boundary. The matrix $\mathbf{b}_s$ describes the discretized form of the boundary conditions around the obstacle. Due to the variational formulation and the application of Lagrange multipliers, no singularities are introduced from such constraint conditions.

The finite element formulation from the variational form of the vorticity transport equation, in Eq. (4), results in a system of first-order nonlinear ordinary differential equations

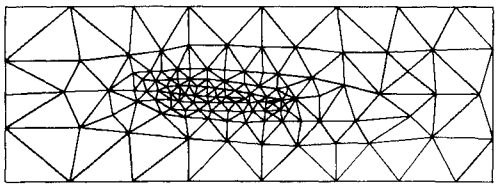

Fig. 1 The finite element gridwork.

$$\begin{bmatrix}\mathbf{S}_\omega & \mathbf{b}_\omega\\ \mathbf{b}_\omega^t & \mathbf{0}\end{bmatrix}\begin{bmatrix}d\mathbf{W}/dt\\ \boldsymbol{\delta}_\omega\end{bmatrix} = \begin{bmatrix}\mathbf{h}_\omega\\ \mathbf{e}_\omega\end{bmatrix} \tag{8}$$

The matrix $\mathbf{S}_\omega$ accounts for the coupling between the nodal accelerations through a consistent variational formulation. $\mathbf{h}_\omega$ includes both the viscous and convection terms in the vorticity transport equation and can be written as follows:

$$\mathbf{h}_\omega = [\mathbf{T}_{sv}+\mathbf{T}_{sc}(\mathbf{u})]\mathbf{W} \tag{9}$$

The derivation of the $\mathbf{h}_\omega$ vector in finite element form is described in detail in Refs. 13 and 14. Matrices $\mathbf{b}_\omega$ and $\mathbf{e}_\omega$ were derived for describing the vorticity boundary conditions at the airfoil boundary. $d\mathbf{W}/dt$ is the time derivate of the instantaneous vorticity field for a given velocity field and a set of boundary conditions. Once this vector is calculated from Eq. (8), a numerical integration technique can be chosen to integrate with respect to time for obtaining results with desired accuracy. The errors in the "time-delay" can be related to the type of the numerical integration technique and the time step. Of course, the nonlinearity in the convection terms in Eq. (9) and the accuracy of the boundary conditions in matrix $\mathbf{b}_\omega$ determine the accuracy of the solution.

Computational Considerations

The solution of the vorticity transport equation requires the numerical integration of the nonlinear discrete system of Eq. (8) and the determination of the velocity field at each time step from Eq. (7). Both Eqs. (7) and (8) are discretized in space and Eq. (8) is also discretized with respect to time. The accuracy and stability of the system of equations will be considered in two parts: in the discretization process and in the solution of the equations. The importance of the viscous and convective terms and the airfoil boundary conditions will be evaluated for both parts.

Accuracy and stability of the solution of the Navier-Stokes equation have been studied using the finite-difference method, when the entire system was represented by a unified molecule in space and time.[6] The application of the finite element method in reducing the vorticity transport equation to a system of ordinary differential equations in time and the separate determination of the velocity field in terms of vorticities enable further simplification of the accuracy and stability problem. In the following, the discretization and solution of each of the Eqs. (7) and (8) are discussed.

Determination of the Velocity Field

For a given vorticity distribution, the velocity field can be determined from the solution of Eq. (7) in the following form:

$$\boldsymbol{\Psi} = \mathbf{q}_s - \mathbf{r}_s(\mathbf{b}_s^t\mathbf{r}_s)^{-1}(\mathbf{b}_s^t\mathbf{q}_s - \mathbf{e}_s) \tag{10}$$

where

$$\mathbf{q}_s = \mathbf{S}_s^{-1}\mathbf{h}_s \tag{11}$$

$$\mathbf{r}_s = \mathbf{S}_s^{-1}\mathbf{b}_s \tag{12}$$

In this form, the boundary conditions for the airfoil can be treated separately and compared with the effects of the surround-

ing vorticity field. Both Eqs. (11) and (12) require the solution of a system of algebraic equations, where $\mathbf{S}_s$ represents the free-stream flow in a viscous fluid without the disturbances of the airfoil. The accuracy of the solution vector Ψ depends both on the conditioning of matrix $\mathbf{S}_s$ and the effects of matrix $\mathbf{b}_s$ on $\mathbf{S}_s$. The properties of matrix $\mathbf{S}_s$ will be discussed first.

$\mathbf{S}_s$ is a positive-definite, symmetric matrix representing the discrete form of the Laplace operator ∇^2. There have been several investigations of the accuracy of solutions of equations in the form

$$\mathbf{S}_s\mathbf{X} = \mathbf{R} \tag{13}$$

using both finite element and finite-difference methods. This problem is the well-known torsion problem in solid mechanics. Pian[16] has discussed the advantages of the finite element method in comparison with finite-difference methods in the analysis of torsion of a rectangular prism. He also presented the accuracy of numerical results obtained from different gridworks using both methods.

In the solution of Eq. (13) the relative errors $\Delta\mathbf{X}$ in the solution vector $\mathbf{X}$, due to perturbations $\Delta\mathbf{S}_s$, can be related as

$$\frac{\|\Delta\mathbf{X}\|}{\|\mathbf{X}\|} \leq N(\mathbf{S}_s)\frac{\|\Delta\mathbf{S}\|}{\|\mathbf{S}\|} + \frac{\|\Delta\mathbf{R}\|}{\|\mathbf{R}\|} \tag{14}$$

where $N(\mathbf{S}_s)$ is the conditioning number of matrix $\mathbf{S}_s$. For a positive-definite matrix

$$N(\mathbf{S}_s) = \mu_{\max}/\mu_{\min} \tag{15}$$

Kelsey, Lee, and Mak[17] have shown that the conditioning number for matrix $\mathbf{S}_s$ in a rectangular plane is proportional to n^2, where n is the number of elements on one side of the rectangular gridwork. The conditioning number remains proportional to n^2, whether matrix $\mathbf{S}_s$ is formulated using a higher-order finite element or finite-difference approximation. This also applies to one-, two-, and three-dimensional formulation of the ∇^2 operator. The advantage of using a higher-order approximation function becomes apparent, since the numerical errors will increase proportionally with the number of elements. A major advantage of the finite element method is the simplicity in developing higher-order elements to increase the accuracy of the solution without increasing the conditioning number. Although the application of a more refined mesh around the obstacle increases the conditioning number, one can obtain quite accurate results from matrix $\mathbf{S}_s$ for the gridwork in Fig. 1 by using a third-order approximation of the variation of stream functions over each triangular element.[13] It should be noted that the solution of Poisson's equation using a "displacement method" is "stiffer"[17] than the exact solution and the eigenvalues of matrix $\mathbf{S}_s$ are an upper bound to the continuous system, while the velocities converge from below.

The next consideration is the importance of the boundary conditions around the obstacle. We can analyze this effect from a modal decomposition of matrix $\mathbf{S}_s$ as

$$S_{sij} = \mu_k p_{ik} p_{jk} \tag{16}$$

where μ_k are the eigenvalues and p_{ik} are the modes. We can normalize the modes as

$$p_{jk}p_{jm} = \begin{cases} 1, & k = m \\ 0, & k \neq m \end{cases} \tag{17}$$

from which the inverse of matrix $\mathbf{S}_s$ can be written

$$S_{sij}^{-1} = (1/\mu_k)p_{ik}p_{jk} \tag{18}$$

Substituting Eq. (17) into Eq. (9) and multiplying by p_{ij}, Eq. (9) can be written as

$$p_{ij}\psi_i = \frac{\mu_m}{\mu_j\mu_k}\frac{\theta_{mj}\theta_{mk}}{\theta_{mm}}\beta_k + \frac{\mu_m}{\mu_j}\frac{\theta_{jm}\theta_{km}}{\theta_{mm}}\tau_k \tag{19}$$

where

$$\alpha_{jk} = p_{ij}b_{ik} \tag{20}$$

$$\beta_j = p_{ij}h_{si} \tag{21}$$

$$e_{sj} = \alpha_{ij}\tau_i \tag{22}$$

$$\theta_{ij} = \alpha_{ik}\alpha_{jk} \tag{23}$$

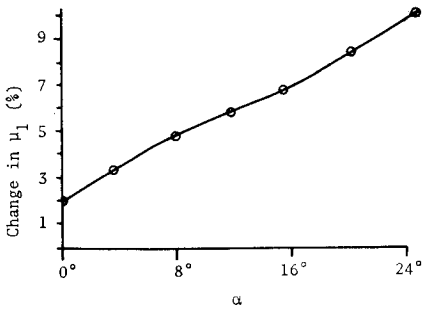

Fig. 2 Variation of the largest eigenvalue, μ_1, with the boundary conditions of NACA 0012 airfoil at different angles of attack.

α_{jk} represent the effect of each boundary condition on the airfoil in terms of the mode p_{ij}. Similarly β_j is the component of the vorticity field and e_{sj} represent the component of the moving airfoil boundary conditions in each mode. In this manner, the velocity-vorticity relationship can be approximated in terms of a few degrees of freedom.

For a stationary airfoil, Eq. (19) can be written for a one-degree-of-freedom system as

$$p_{ij}\psi_j = (1-\theta_{11})/\mu_1 \tag{24}$$

It appears then that the largest eigenvalue will become

$$\mu_1/(1-\theta_{11}^2) \tag{25}$$

Therefore, for obstacles with different geometry we can expect changes in the conditioning number due to boundary conditions. Variation of the largest eigenvalue for the NACA 0012 airfoil, at different angles of attack, is shown in Fig. 2 for the finite element gridwork of Fig. 1. For the case of an oscillating airfoil, the eigenvalues will again change, depending on the instantaneous motion of the airfoil and its position. Stability of flow for a particular obstacle shape and obstacle motion can be studied from these equations.

Numerical Integration of the Vorticity Transport Equation

There have been numerous investigations of the accuracy and stability of the solution of the vorticity transport equation based on finite-difference formulations.[7] First-, second-, and fourth-order finite-difference approximations of the convective terms in this equation were discussed by Fromm.[9] Fromm[1] has also discussed certain basic instability problems, for example, when a first-order centering in time and second-order centering in space is used. However, the finite-difference formulations do not allow separate treatments of convective and viscous terms and the boundary conditions. Using the finite element formulation of Eq. (8), one can give a more systematic analysis of the accuracy and stability problem.

The vorticity transport equation can be integrated numerically, while at each time step, the time derivative of vorticities are determined from Eq. (8) and the instantaneous velocity field is determined from Eq. (7). The solution of matrix Eq. (8) can be written as follows:

$$\mathbf{S}_\omega\, d\mathbf{W}/dt = \mathbf{h}_\omega - \mathbf{b}_\omega(\mathbf{b}_\omega{}^t\mathbf{r}_\omega)^{-1}(\mathbf{b}_\omega{}^t\mathbf{q}_\omega - \mathbf{e}_\omega) \tag{26}$$

where

$$\mathbf{q}_s = \mathbf{S}_\omega{}^{-1}\mathbf{h}_\omega \tag{27}$$

$$\mathbf{r}_\omega = \mathbf{S}_\omega{}^{-1}\mathbf{b}_\omega \tag{28}$$

From Eq. (9), Eq. (26) can be written in a compact form as

$$\mathbf{S}_\omega\, d\mathbf{W}/dt = \mathbf{B}(\mathbf{u})\mathbf{W} + \mathbf{C} \tag{29}$$

where

$$\mathbf{B}(\mathbf{u}) = [\mathbf{I} - \mathbf{b}_\omega(\mathbf{b}_\omega{}^t\mathbf{r}_\omega)^{-1}\mathbf{b}_\omega{}^t\mathbf{S}_\omega{}^{-1}][\mathbf{T}_{\omega v} + \mathbf{T}_{\omega c}(\mathbf{u})] \tag{30}$$

and

$$\mathbf{C} = \mathbf{b}_\omega(\mathbf{b}_\omega{}^t\mathbf{r}_\omega)^{-1}\mathbf{e}_\omega \tag{31}$$

$\mathbf{T}_{\omega v}$ in Eq. (9) describes the effect of viscosity in the velocity field surrounding the airfoil. Since this matrix corresponds to the discretized form of the viscous term in Eq. (1), it is positive-definite. $\mathbf{T}_{\omega c}$ matrix consists of nonlinear convective terms. The properties of $\mathbf{B}(\mathbf{u})$ depend on the relative magnitudes of the viscous and convective terms in $\mathbf{T}_{\omega v}$ and $\mathbf{T}_{\omega c}$ matrices together with the airfoil boundary conditions in the first portion of the right-hand side in Eq. (30).

Using a forward difference approximation in time, which corresponds to the application of Euler's numerical integration technique for the system in Eq. (29), the stability of the integration depends on the maximum eigenvalue of the following system

$$\lambda \mathbf{S}_\omega \mathbf{X} = \mathbf{B}\mathbf{X} \tag{32}$$

The maximum eigenvalue will depend on the relative importance of viscous and convective terms and the boundary conditions over the airfoil, as can be seen in Eqs. (29–31). The discretization errors will also change the eigenvalues as discussed previously. The numerical damping vs the physical damping can be analyzed in terms of these discretization errors and the errors from the numerical integration techniques as a function of the largest eigenvalue λ. The condition for stability for the system in Eq. (29), from a first-order numerical integration technique, becomes

$$\Delta t < 2/\lambda_{\max} \tag{33}$$

if all eigenvalues are real and positive. This discussion can be extended to higher-order numerical integration techniques. Generally, the upper limit of $\lambda_{\max}\Delta t$ varies between values of 1 to 6 for explicit numerical integration techniques.[18] Stable results can be obtained for a sufficiently small time step. Accuracy depends again on the time step and the order of the numerical integration procedure. Another advantage of the finite element formulation is the convenient use of implicit numerical integration techniques. Stability problems are eliminated and accuracy becomes a function of the number of iterations at each step.

To evaluate the accuracy and stability problems encountered in the explicit numerical integration techniques, one has to investigate the maximum eigenvalue of the system in Eq. (8). Based on the finite element formulation of the system, an upper bound to the maximum eigenvalue can be obtained[19] as

$$\lambda_{\max} = \frac{\mathbf{X}^t\mathbf{B}\mathbf{X}}{\mathbf{X}^t\mathbf{S}_\omega\mathbf{X}} \leq \left|\frac{\mathbf{X}^t\mathbf{B}\mathbf{X}}{\mathbf{X}^t\mathbf{S}_\omega\mathbf{X}}\right|^e_{\max} \tag{34}$$

The highest eigenvalue of the system can then be approximated by considering the maximum eigenvalue of each of the elements. By assuming a linear variation of vorticities and velocities over each finite element, the variational formulation of Eq. (8) yields the following relationship

$$\left\{\begin{bmatrix} \frac{vy_{23}}{4\Omega}+\frac{1}{24}(2u_1+u_2+u_3) \\ \frac{vy_{31}}{4\Omega}+\frac{1}{24}(u_1+2u_2+u_3) \\ \frac{vy_{12}}{4\Omega}+\frac{1}{24}(u_1+u_2+2u_3) \end{bmatrix}[y_{23}y_{31}y_{12}] + \begin{bmatrix} \frac{vx_{32}}{4\Omega}+\frac{1}{24}(2v_1+v_2+v_3) \\ \frac{vx_{13}}{4\Omega}+\frac{1}{24}(v_1+2v_2+v_3) \\ \frac{vx_{21}}{4\Omega}+\frac{1}{24}(v_1+v_2+2v_3) \end{bmatrix}[x_{32}x_{13}x_{21}] - \frac{\lambda_i\Omega}{12}\begin{bmatrix} 2&1&1 \\ 1&2&1 \\ 1&1&2 \end{bmatrix}\right\}\begin{bmatrix}\omega_1\\ \omega_2\\ \omega_3\end{bmatrix} = \mathbf{0} \tag{35}$$

One can evaluate stability problems in terms of viscous and convective terms and the boundary conditions from the following simple model. If we assume a triangular finite element in the freestream flow as shown in Fig. 3, the eigenvalues of this element become

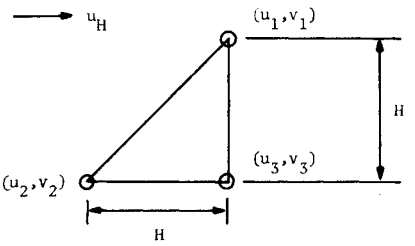

Fig. 3 A triangular element in the finite element gridwork.

$$\lambda_i = 0, \gamma, 3\gamma \quad \text{where} \quad \gamma = 12\nu/H^2 \tag{36}$$

Without any boundary conditions, the stability of Eq. (8) depends only on the viscous terms and the size of the finite element. Convective terms do not cause instability in the freestream.

If we assume that the triangle in Fig. 3 is resting on a flat plate boundary and the velocities at the nodes are $u_1 = u_H$, $u_2 = u_3 = v_1 = v_2 = v_3 = 0$, then the eigenvalues become

$$\lambda_1 = 0, \quad \lambda_{2,3} = 2\gamma \pm \{\gamma[\gamma - (\eta/4)]\}^{1/2} \tag{37}$$

where

$$\eta = 4u_H/H \tag{38}$$

and

$$Re^e = u_H H/\gamma \tag{39}$$

Equation (37) shows that, if

$$\eta > 4\gamma \quad \text{or} \quad Re^e > 12 \tag{40}$$

then the eigenvalues have an imaginary part. In this case, an oscillatory behavior in the solution of vorticity transport equations is expected. The damping of the oscillations will be proportional to the viscous terms represented by γ in Eq. (37).

If the parabolic distribution of velocities is assumed over a triangular element, the eigenvalues on the boundary for this element become

$$\lambda_1 = 0, \quad \lambda_{2,3} = 2\gamma \pm [\gamma^2 - \tfrac{3}{10}\gamma\eta]^{1/2} \tag{41}$$

In such cases the oscillatory behavior starts when

$$Re^e > 10 \tag{42}$$

Finally, a case was considered when the velocities at the nodes of the finite element triangle in Fig. 3 are $u_1 = v_1 = u_H$ and $u_2 = u_3 = v_2 = v_3 = 0$. In this case the eigenvalues are found to be real and equal to

$$\lambda_1 = 0, \quad \lambda_2 = 3\gamma + (\eta/2\gamma), \quad \lambda_3 = \gamma + \tfrac{7}{24}\eta \tag{43}$$

The eigenvalues are linearly proportional to the velocity at the upper node of the triangle. At high Reynolds numbers, the condition for stability in Eq. (33) becomes

$$\Delta t \leq 2H/u_H \tag{44}$$

A higher-order approximation of velocities changes this condition only slightly. For a second-order variation of velocities, the condition for stability becomes

$$\Delta t \leq \tfrac{5}{3}H/u_H \tag{45}$$

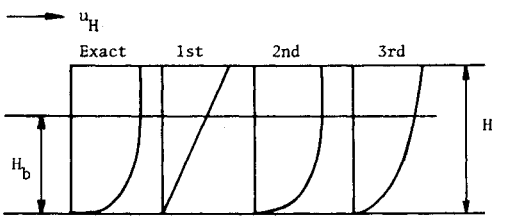

Fig. 4 Approximation of the boundary-layer velocity distribution along a flat plate with first-, second-, and third-order approximation functions.

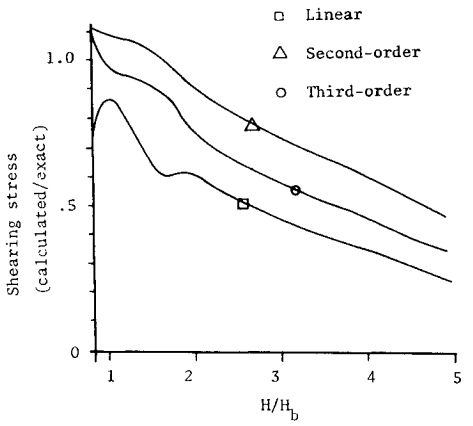

Fig. 5 Comparison of the accuracy of approximations of the boundary layer with first-, second-, and third-order polynomials.

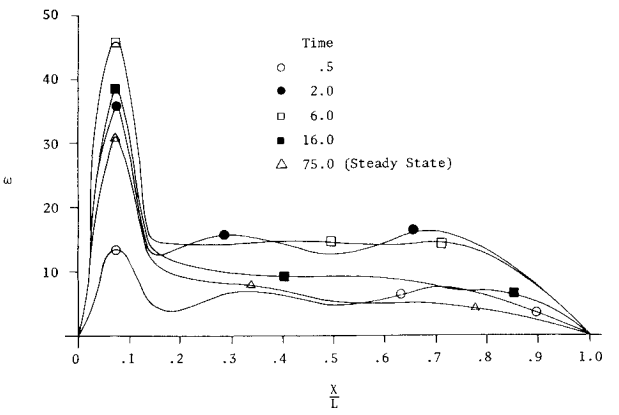

Fig. 7 Vorticity distribution over the airfoil ($\alpha = 0°$, $Re = 10^3$) at different time intervals.

As can be seen from Eqs. (44) and (45), while the accurate representation of the boundary layer requires smaller elements, Δt must be reduced accordingly; however, by using higher-order finite elements the same degree of accuracy can be achieved without causing stability problems.

Accuracy of the Representation of the Boundary Layer

An important consideration for the accuracy and stability of solutions of the Navier-Stokes equation is the accurate representation of the boundary layer. At high Reynolds numbers, as the boundary layer becomes thinner, the design of the finer mesh around the obstacle becomes impractical. This difficulty can again be dealt with by using higher-order finite elements for the velocity distribution around the obstacle. As it was discussed previously, the finite element solution of Eq. (7) is a stiffer solution, which gives lower values of the velocities around the obstacle. The thickness of the boundary layer may be comparable or smaller than the height of a finite element triangle as shown in Fig. 4. If we assume that the base of the triangle rests on a flat plate, the boundary layer is approximated by the velocity distribution of one triangle. In Fig. 5, the ratios of the shear stresses on the plate boundary are compared when this triangular element is represented by linear, second-order, and third-order approximation functions.[20] Second-order approximation gives stiffer results than the third-order approximation function. From these results one can observe that a higher-order approximation function improves the accuracy of the solution considerably.

Sample Problem: Analysis of Flow Around a NACA 0012 Airfoil

Results obtained from the finite element analysis of flow around a NACA 0012 airfoil are presented to illustrate various computational aspects of the analysis. Several examples of such analyses are given in Ref. 21.

The pressure and vorticity distribution at the boundary of the airfoil is plotted as a function of time in Figs. 6 and 7. The vorticities were assumed to be zero at the start of the numerical integration. This assumption corresponds to a sudden start of the flow with a jump from zero to a maximum velocity. At the initial steps of the integration, high values of pressure are obtained due to this starting condition. The pressure over the entire airfoil surface then decreases uniformly to a steady state. The vorticity field, however, increases suddenly due to the sudden start of the flow. An underrelaxation factor was used to eliminate the instabilities around the airfoil during the first few steps of the numerical integration. After a maximum value is reached the vorticities then also decrease to a steady state.

As can be seen from Figs. 8 and 9, larger time steps do slow down the rate of convergence of the solution. This behavior can be explained for the system in Eq. (25), where the rate of convergence is proportional to the largest eigenvalue and the time step. In the case of divergent results, the vorticity distribution started from zero and increased continuously. One was able to

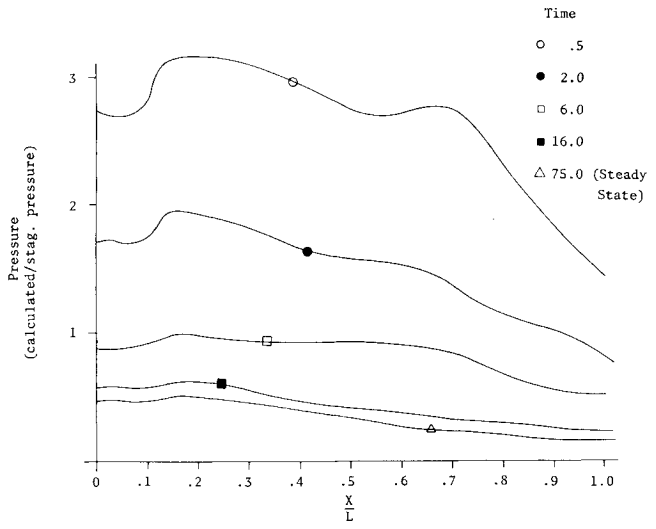

Fig. 6 Pressure distribution over the airfoil ($\alpha = 0°$, $Re = 10^3$) at different time intervals.

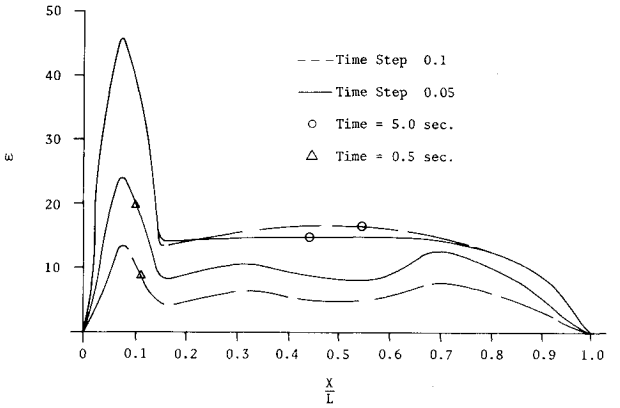

Fig. 8 Vorticity distribution over the airfoil ($\alpha = 0°$, $Re = 10^3$) at different time intervals using different time steps for numerical integration.

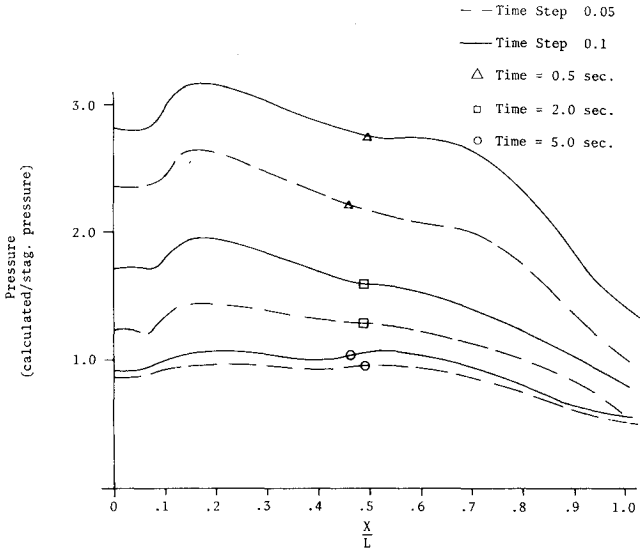

Fig. 9 Pressure distribution over the airfoil ($\alpha = 0°$, $Re = 10^3$) at different time intervals using different time steps for numerical integration.

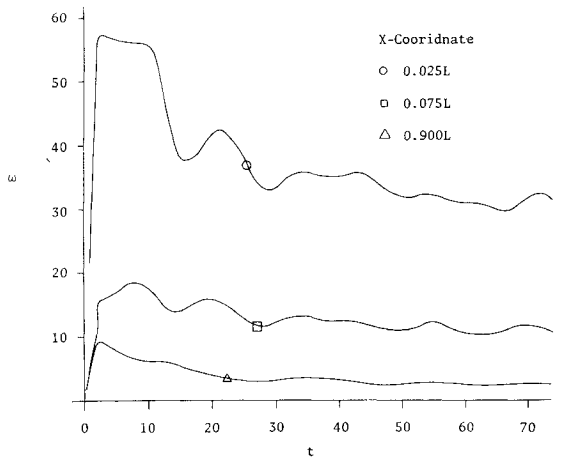

Fig. 12 Variation of vorticities during the numerical integration of the vorticity transport equation starting from zero vorticity distribution ($\alpha = 0°$, $Re = 10^3$).

detect the divergence at a particular point on the surface of the airfoil. Figures 10 and 11 show the vorticity values at two points around the airfoil at $Re = 10^5$. As the numerical integration was advanced, an oscillatory divergence was obtained starting from the obstacle boundary. The time lag between these two points can be observed from these figures.

Figures 12 and 13 show the convergence to a steady state at several points on the airfoil. While the convergence is rather steady at the trailing edge of the airfoil, at the leading edge, where the curvature is greater, there is an oscillatory convergence. The same results are reflected in the pressure diagrams. The convergence was slower at the leading edge of the airfoil, as can be seen from Figs. 14 and 15. At larger time steps, the vorticities were diffusing with a slower rate.

A computational experiment is presented in Fig. 16 demonstrating the importance of numerical integration techniques. A point vortex of unit magnitude was introduced at the upstream of the airfoil and the vorticity transport equations were integrated using Euler, Fourth-order Runge-Kutta, and Fourth-order Milne Predictor-corrector techniques. At the point where the vortex was introduced, the vorticities decreased uniformly. The Euler method showed a stiffer behavior. On the other hand, at a point close to the airfoil, results with the Predictor-corrector method, which is known to be sensitive to instabilities, became unstable. As can be seen from these results, such behavior is related to the time discretization and the effects of the boundary conditions on the airfoil.

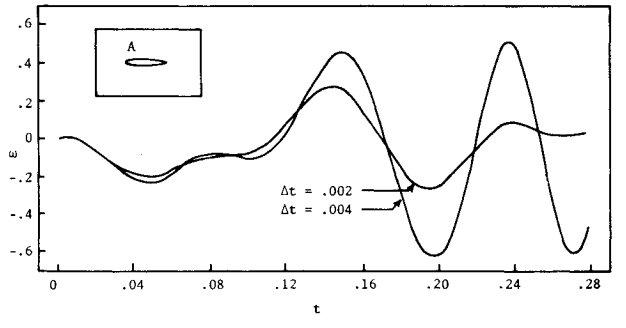

Fig. 10 Accuracy and stability of the numerical integration of the vorticity transport equation for a point (A) upstream of the airfoil ($\alpha = 0°$, $Re = 10^5$).

Discussion

The preceding presentation described some of the sources of computational difficulties encountered in the application of the

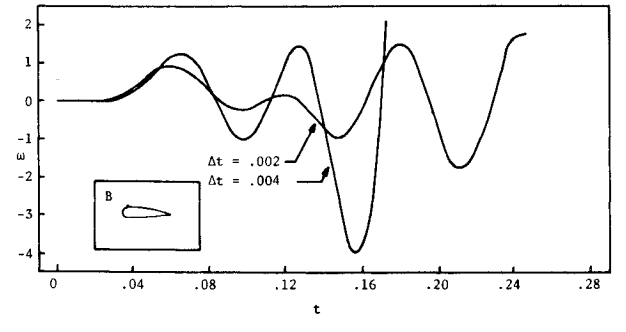

Fig. 11 Accuracy and stability of the numerical integration of the vorticity transport equation for a point (B) near the airfoil ($\alpha = 0$, $Re = 10^5$).

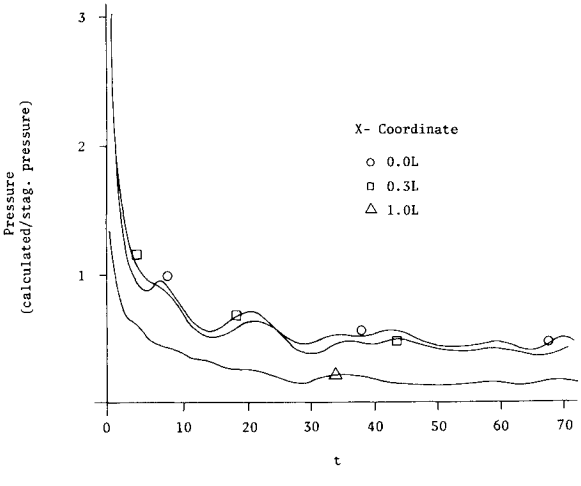

Fig. 13 Variation of pressures during the numerical integration of the vorticity transport equation starting from zero vorticity distribution ($\alpha = 0°$, $Re = 10^3$).

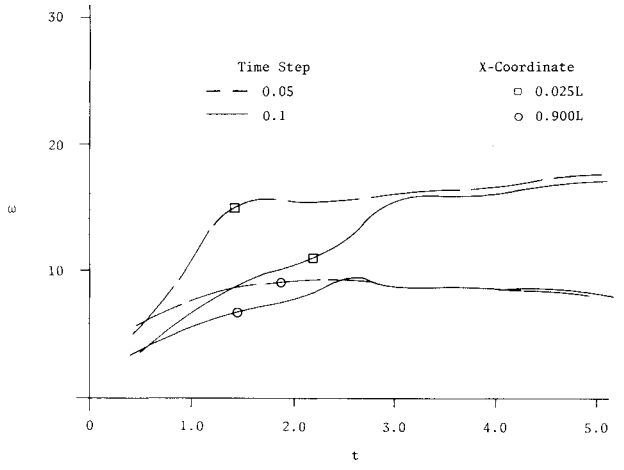

Fig. 14 Determination of the steady-state values of vorticities using different time steps in the numerical integration ($\alpha = 0°$, $Re = 10^3$).

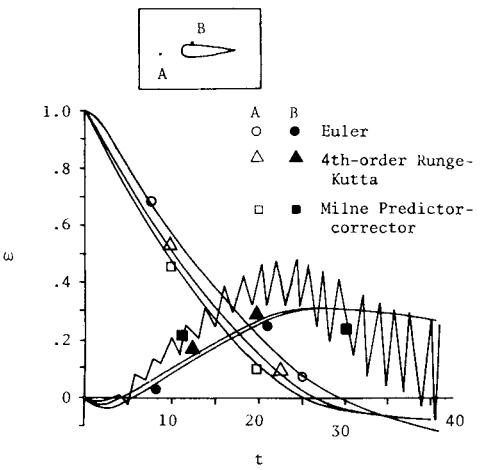

Fig. 16 Variation of the vorticities at two points around the airfoil as calculated by different numerical integration techniques ($\alpha = 0°$, $Re = 100$).

finite element method for the analysis of flow problems. Available mathematical tools for dealing with such difficulties were also described. In comparison with finite-difference techniques, finite-element solutions of flow problems prove to be more flexible and efficient in treating accuracy and stability problems. Considering these sources of errors, decisions can be made in choosing required parameters for obtaining accurate and stable results. The important computational considerations are summarized as follows.

For the finite-element analysis, the obstacle and the surrounding flowfield are represented by a discrete system of triangular elements similar to the one shown in Fig. 1. The dimensions of the rectangular space containing the obstacle and the surrounding flow must be specified in a manner to adequately satisfy the freestream conditions. The oscillating obstacle should be described by a sufficient number of triangles. It has also been shown that the use of higher-order approximation functions of the velocity field improves the accuracy at the boundary layer without introducing additional numerical errors.

Once the finite element model representing the vorticity transport equation is formulated, it can be integrated as a system of ordinary differential equations. The stability and accuracy of this system depend on the largest eigenvalue, which is a function of the finite element gridwork (number of elements and size and position of the elements) and flow parameters (Reynolds number, boundary layer, etc.) around the obstacle. At higher Reynolds numbers, the time step of the numerical integration and the numerical integration procedure must be chosen in a manner to obtain accurate and stable results. It becomes more advantageous to represent the boundary layer using higher-order approximation functions and to decrease the time step, since smaller finite elements would introduce numerical errors in determining the velocity field. A finer mesh must be used at regions where the velocity gradient becomes larger.

The application of higher-order numerical integration techniques improves the accuracy and stability without unduly complicating the computation. By using Runge-Kutta and Predictor-corrector type of numerical integration techniques, stability problems can be controlled and accuracy limits can be set. In Eq. (29) matrix $\mathbf{S}_\omega$ is a positive-definite symmetric matrix. Matrix **B** consists of two parts: viscous terms, which also yield a positive-definite matrix, and convective terms. As the convective terms become more pronounced, depending on the obstacle geometry, the eigenvalues may have both real and imaginary components. Depending on such characteristics of the system of equations, the numerical integration techniques have to be modified.

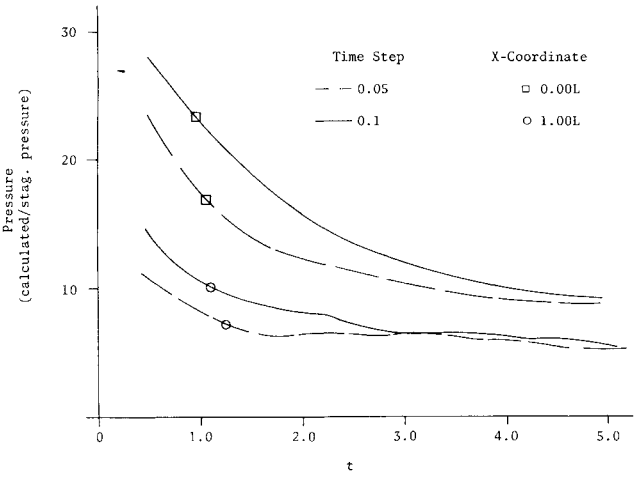

Fig. 15 Determination of the steady-state values of pressures using different time steps in the numerical integration ($\alpha = 0°$, $Re = 10^3$).

References

[1] Fromm, J. E., "A Method for Computing Nonsteady, Incompressible, Viscous Fluid Flows," Rept. LA-2910, Sept. 1963, Los Alamos Scientific Lab., Los Alamos, N. Mex.

[2] Spalding, D. B., "Numerical Methods in Fluid Mechanics and Heat Transfer," *Computer Aided Engineering*, edited by G. M. L. Gladwell, University of Waterloo, Waterloo, Ontario, Canada, 1970, p. 509.

[3] Takami, H. and Keller, H. B., "Steady Two-Dimensional Viscous Flow of an Incompressible Fluid past a Circular Cylinder," *The Physics of Fluids*, Suppl. II, Vol. 12, No. 12, Dec. 1969, p. 51.

[4] Thoman, D. C. and Szewczyk, A. A., "Time-Dependent Viscous Flow over a Circular Cylinder," *The Physics of Fluids*, Suppl. II, Vol. 12, No. 12, Dec. 1969, p. 76.

[5] Takaisi, Y., "Numerical Studies of a Viscous Liquid past a Circular Cylinder," *The Physics of Fluids*, Suppl. II, Vol. 12, No. 12, Dec. 1969, p. 86.

[6] Noh, W. F. and Protter, M. H., "Difference Methods and the Equations of Hydrodynamics," *Journal of Mathematics and Mechanics*, Vol. 12, No. 2, 1963, p. 149.

[7] Richtmyer, R. D. and Morton, K. W., *Difference Methods for Initial-Value Problems*, 2nd ed., Interscience Publishers, New York, 1967.

[8] Cheng, Sin-I, "Accuracy of Difference Formulation of Navier-Stokes Equations," *The Physics of Fluids*, Suppl. II, Vol. 12, No. 12, Dec. 1969, p. 34.

[9] Fromm, J. E., "Practical Investigation of Convective Difference Approximations of Reduced Dispersion," *The Physics of Fluids*, Suppl. II, Vol. 12, No. 12, Dec. 1969, p. 3.

[10] Moretti, G., "Importance of Boundary Conditions in the Numerical Treatment of Hyperbolic Equations," *The Physics of Fluids*, Suppl. II, Vol. 12, No. 12, Dec. 1969, p. 13.

[11] Cheng, R. T.-S., "Numerical Solution of the Navier-Stokes Equations by the Finite Element Method," *The Physics of Fluids*, Vol. 15, No. 12, Dec. 1972, pp. 2093–2105.

[12] Taylor, C. and Hood, P., "A Numerical Solution of the Navier-Stokes Equations Using the Finite Element Technique," *International Journal of Computers and Fluids*, Vol. 1, No. 1, 1973, pp. 73–100.

[13] Bratanow, T., Ecer, A., and Kobiske, M., "Finite Element Analysis of Unsteady Incompressible Flow Around an Oscillating Obstacle of Arbitrary Shape," *AIAA Journal*, Vol. 11, No. 11, Nov. 1973, pp. 1471–1477.

[14] Bratanow, T., Ecer, A., and Kobiske, M., "Numerical Calculations of Velocity and Pressure Distribution Around Oscillating Airfoils," CR-2368, March 1974, NASA.

[15] Bratanow, T. and Ecer, A., "Suitability of the Finite Element Method for Analysis of Unsteady Flow Around Oscillating Airfoils," International Conference on Numerical Methods in Fluid Dynamics, Univ. of Southampton, Southampton, England, Sept. 26–28, 1973.

[16] Pian, T. H. H., "Variational Formulations of Numerical Methods in Solid Continua," *Computer Aided Engineering*, edited by G. M. L. Gladwell, University of Waterloo, Waterloo, Ontario, Canada, 1970, p. 421.

[17] Kelsey, S., Lee, K. N., and Mak, C. K. K., "The Condition of Some Finite Element Coefficient Matrices," *Computer Aided Engineering*, edited by G. M. L. Gladwell, University of Waterloo, Waterloo, Ontario, Canada, 1970, p. 267.

[18] Lapidus, L. and Seinfeld, J. H., *Numerical Solution of Ordinary Differential Equations*, Academic Press, New York, 1971.

[19] Tong, P., "On the Numerical Problems of the Finite Element Methods," *Computer Aided Engineering*, edited by G. M. L. Gladwell, University of Waterloo, Waterloo, Ontario, Canada, 1970, p. 539.

[20] Schlichting, H., *Boundary Layer Theory*, 6th Ed., McGraw-Hill, New York, 1968.

[21] Bratanow, T. and Ecer, A., "Computational Considerations in Application of the Finite Element Method for Analysis of Unsteady Flow Around Airfoils," *Proceedings of AIAA Computational Fluid Dynamics Conference*, Palm Springs, Calif., July 19–20, 1973, p. 109.